scientific reports

Check for updates

OPEN

PDZK1 inhibits MRP2-mediated oxaliplatin chemosensitivity in hepatocellular carcinoma

Zeqi Duan[1], Jinyu Li[2,3], Chao Ren[4], Yi Chen[2,3], Duiping Feng[2,3,4], Yanbo Ma[5,6][✉] & Chunjuan Zhao[2,3,4,6][✉]

Recurrence after oxaliplatin chemotherapy is a major challenge in the treatment of advanced hepatocellular carcinoma patients. Differential expression gene analysis and Kaplan-Meier curves were screened biomarkers associated with OXA-treated recurrence in GSE51951, TCGA-LIHC, and Chinese Liver Cancer Atlas databases. We retrospectively collected 39 cases of HCC treated with platinum based drugs at the First Hospital of Shanxi Medical University. Immunohistochemistry was used to analyze the relationship between PDZK1 expression and patient recurrence of HCC. Cell model and subcutaneous transplant tumor model of HCC were established to detect the cell growth ability treated with OXA. Gene Set Enrichment Analysis analysis identified signaling pathways associated with high PDZK1. Co-Immunoprecipition and immunofluorescence experiments were used to explore the potential interaction between PDZK1 and MRP2. We identified that high expression of PDZK1 was associated with OXA resistance and poor prognosis in HCC. PDZK1 promoted the cell viability, migration, and invasion of HCC after OXA treatment in vitro and vivo. MRP2-mediated ABC transporters pathway and bile acid metabolism were significantly activated in the PDZK1 overexpression group of HCC. PDZK1 interacted and co-localized with the carboxyl terminal PDZ binding motif of MRP2. Clinical specimen analysis have shown a positive correlation between the protein levels of PDZK1 and MRP2. Our study identified PDZK1 as a novel biomarker significantly associated with OXA chemosensitivity in HCC. Mechanistically, PDZK1 promoted the OXA sensitivity of HCC by activating the MRP2-mediated signaling pathway.

Keywords Hepatocellular carcinoma, PDZK1, Oxaliplatin, MRP2, Chemosensitivity

Abbreviations

HCC	Hepatocellular carcinoma
OXA	Oxaliplatin
PDZK1	PDZ domain containing 1
MRP2	Multidrug resistance proteins 2
ABCC2	ATP binding cassette subfamily C member 2
TACE	Transarterial chemoembolization
HAIC	Hepatic arterial infusion chemotherapy
TCGA-LIHC	The Cancer Genome Atlas Liver Hepatocellular Carcinoma
CLCA	Chinese Liver Cancer Atlas RFS: Relapse-free survival
AFP	Alpha fetoprotein
CR	Complete response
PR	Partial response
SD	Stable disease
PD	Progressive disease

[1]First Clinical Medical College, Shanxi Medical University, Taiyuan 030001, Shanxi Province, People's Republic of China. [2]Department of Oncological and Vascular Intervention, First Hospital of Shanxi Medical University, Taiyuan 030001, Shanxi Province, People's Republic of China. [3]Shanxi Provincial Clinical Research Center for Interventional Medicine, First Hospital of Shanxi Medical University, Taiyuan 030001, Shanxi Province, People's Republic of China. [4]College of Medical Imaging, Shanxi Medical University, Taiyuan 030001, Shanxi Province, People's Republic of China. [5]Department of Hepatobiliary and Pancreatic Surgery and Liver Transplantation Center, First Hospital of Shanxi Medical University, Taiyuan 030001, Shanxi Province, People's Republic of China. [6]Yanbo Ma and Chunjuan Zhao contributed equally to this work. [✉]email: 15534706968@163.com; zhao.cj@qq.com

CAFs	cancer-associated fibroblasts
ECM	Extracellular matrix
TPTE2P1	Transmembrane phosphoinositide 3-phosphatase and tensin homolog 2 pseudogene 1
PDGFA	Platelet-derived growth factor receptor alpha
SPOCK3/TICN3	Testican-3
VSIG4	V-set and immunoglobulin domain-containing protein 4
lncRNA	Long non-coding RNA

Hepatocellular carcinoma (HCC) is the most common primary liver cancer, which is the third leading cause of cancer-related death worldwide[1]. Chemotherapy through trans-arterial chemoembolization (TACE) and hepatic arterial infusion (HAIC) is currently the main treatment method for advanced hepatocellular carcinoma[2–4]. Oxaliplatin (OXA), as a third-generation platinum based drug, has a positive therapeutic effect on advanced hepatocellular carcinoma[5,6]. The main constraint on platinum based drugs is that some patients are insensitive to their chemotherapy drugs[5,7]. Therefore, understanding the mechanism of insensitivity to oxaliplatin in HCC patients and screening oxaliplatin sensitive patients have important guiding significance for clinical treatment.

The molecular mechanism of OXA chemotherapy insensitivity in HCC has been studied, including cellular metabolism[8], epigenetic modifications[6], cell invasion[9], cell migration[9,10], cell proliferation[11] and cell apoptosis[11]. M2 macrophage polarization can promote OXA chemotherapy mediated resistance in HepG2 cells by affecting cell proliferation and apoptosis ability[11]. High expression of PBK alleviated OXA-induced apoptosis and promoted the migration and invasion of OXA-treated HCC cells[9].

PDZK1, as a scaffold protein, had been considered a promising tumor biomarker in recent years, and its role in the progression of various cancers and chemotherapy resistance had been confirmed[12–15]. Although PDZK1 may act as an oncogene in HCC[16–18], the relationship between PDZK1 and chemotherapy sensitivity to OXA in HCC remains to be studied. PDZK1, also known as NHERF3, is a member of the NHERF family and contains four PDZ domains[12–14]. PDZ protein binds to proteins with PDZ domain-binding motif (PBM) structure through its PDZ domain, thereby affecting the target protein mediated signaling pathway[19–21]. PDZK1 participates in tumor development by interacting with multiple kinds of proteins, including ABCG2, and regulating their activities[12–15].

MRP2, also known as ABCC2, is a member of ATP-binding cassette (ABC) transporters family, play an irreplaceable role in the drug resistance[22,23]. The overexpression of MRP2 contributes to the failure of chemotherapies and symbolizes a great challenge in oncology, associated with the adaptation of tumor cells to anticancer drugs such that these transporters become less effective[24–26]. It is reported that MRP2-induced oxaliplatin resistance prevented NF-kappaB-Nrf2 signaling in colorectal cancer[22,23]. Moreover, as one of the bile acid receptors, MRP2 mediated bile acid metabolism was closely related to HCC malignant progression. In addition, MRP2 contains binding motifs that can bind to PDZ proteins, making it a potential binding protein for PDZK1.

In this study, differentially expressed genes sensitive to OXA-based chemotherapy were screened through OXA-resistant HCC and clinical databases, and it was found that PDZK1 serve as a potential biomarker associated with OXA chemosensitivity. We functionally confirmed that PDZK1 inhibited the chemosensitivity of OXA. In addition, we demonstrated that MRP2, as an interacting protein of PDZK1, was a key molecule insensitive to PDZK1 mediated OXA chemotherapy. Finally, we found a positive correlation between low expression of PDZK1 and OXA chemotherapy response based on TACE and HAIC in clinical samples. In summary, we found that PDZK1 inhibited OXA chemosensitivity in HCC.

Materials and methods

Human specimens

Tissue samples for screening were prospectively obtained from advanced HCC patients who treated with platinum-based drugs (TACE or HAIC) at the First Affiliated Hospital of Shanxi Medical University, from 2019 to 2023. Of the initial cohort, 60 patients were excluded due to diagnoses other than hepatocellular carcinoma. Additionally, 8 patients were removed for not receiving platinum-based chemotherapy, 22 patients were excluded due to loss to follow-up, and 9 patients were omitted due to missing pathological tissue samples, resulting in a final cohort of 39 patients available for analysis. Samples were divided into Response/Non-recurrence (21 patients) and Non-Response/Recurrence (18 patients) groups after the treatment evaluated by mRECIST criterion, and the clinical characteristics are included in Table 1. The use of clinical information in this study was approved by the Ethics Committee of First Affiliated Hospital of Shanxi Medical University, and informed written consent was obtained from all participants. Research involving human research participants have been performed in accordance with the Declaration of Helsinki.

Data availability

The previously published data are openly available in GSE51951 at [https://www.ncbi.nlm.nih.gov/geo/query/acc.cgi?acc=GSE51951]; TCGA-LIHC at [https://www.cbioportal.org/study/summary?id=lihc_tcga]; CLCA project at [https://www.cbioportal.org/study/summary?id=hcc_clca_2024].

DEGs analysis

The results of DEGs were generated using an online analysis platform [https://www.bioinformatics.com.cn]. The filtering criteria were set to $|$ fold change $| \geq 1.5$ and $p < 0.001$. Comparing oxaliplatin-resistant MHCC97H ($n = 3$) and control MHCC97H ($n = 3$) from GSE51951 database and the HCC group ($n = 47$) and paired non-tumor group ($n = 47$) in the TCGA-LIHC database. Co-expressed DEGs obtained from GSE51951 and TCGA-LIHC by VENNY 2.1.0.

Parameters	Total ($n = 39$)	Non-recurrence ($n = 21$)	Recurrence ($n = 18$)	P value
Demographic parameters				
Age (years), mean ± SD	63.1 ± 10.7	67.4 ± 9.6	57 ± 9	< 0.001***
Male sex, n(%)	32 (82.1%)	17 (81%)	15 (83.3%)	0.847
TNM-stage, n(%)				
I, II	16 (33.3%)	12 (57.1%)	4 (22.2%)	0.027*
III, IV	23 (66.7%)	9 (42.9%)	14 (77.8%)	
AFP (ng/ml), n(%)				
< 200	23 (66.7%)	14 (66.7%)	9 (50%)	0.291
> 200	16 (33.3%)	7 (33.3%)	9 (50%)	
Hepatitis B virus, n(%)				
Positive	24 (61.5%)	9 (42.9%)	15 (83.3%)	0.01*
Negative	15 (38.5%)	12 (57.1%)	3 (16.7%)	
Tumor grade, n(%)				
G1, G2	19 (48.7%)	12 (57.1%)	7 (38.8%)	0.906
G3	3 (7.7%)	2 (9.6%)	1 (5.6%)	
Gx	17 (43.6%)	7 (33.3%)	10 (55.6%)	

Table 1. Baseline characteristics of patients. *p<0.05,**p<0.01,***p<0.001.

Gene set enrichment analysis (GSEA)

Gene Set Enrichment Analysis (RRID: SCR_003199) was used to screen the differential gene sets between the PDZK1-high and PDZK1-low groups in the TCGA-LIHC database. The bubble plot displayed the top 10 differential genes sets. *KEGG_ABC_TRANSPORTERS* (M11911A) and *HALLMARK_BILE_ACID_METABOLISM* (M5948) was downloaded from https://www.gsea-msigdb.org/gsea/index.jsp. The statistically significant enrichment was defined as a false discovery rate (FDR) < 0.25.

Cell lines and cell culture

The liver cancer cell lines Huh-7 (RRID: CVCL_0336), Hep-G2 (RRID: CVCL_0027) were kindly provided by Wuhan Pricella Biotechnology Co.,Ltd. HEK293T (RRID: CVCL_0063) was purchased from Abcell (Beijing, China). All cell lines were correctly identified by Short tandem repeat (STR) profiling and were tested negative for mycoplasma contamination. Cells were maintained in Dulbecco's Modified Eagle medium (DMEM; Thermo Fisher Scientific, Waltham, USA) supplemented with 10% fetal bovine serum (FBS; Cell-box, Hunan, China) and 1% penicillin/streptomycin solution at 37 °C in 5% CO2.

Plasmid constructions and RNA interference (RNAi) and transfection

Constructs of plasmid (pcDNA3.1(+)-PDZK1, pcDNA3.1(+)-3*HA-PDZK1, pcDNA3.1(+)-3*Flag-ABCC2 and pcDNA3.1(+)-3*Flag-ABCC2(delAA1542-1545) were bought from PPL (Public Protein/Plasmid Library, China). The siRNA targeting PDZK1 (Forward: 5'-GGUGAAUGUGCUAGAUGAAUT-3', Reverse: 5'-UUCAU CUAGCACAUUCACCTT-3'), MRP2 (Forward: 5'-GGAAGAAAGAGCUCAAGAATT-3', Reverse: 5'-UUCU UGAGCUCUUUCUUCCTT) were synthesized by Hysigen Biology. The plasmid and siRNA were transfected into HepG2 cells by LipofectamineTM3000 (Thermo Fisher Scientific, Waltham, USA) according to the manufacturer's instructions. After transfection for 48 h, western-blotting assay were performed to evaluate the knockdown efficiency. Lenti-SFFV-PDZK1-3FLAG-IRES-PURO-WPRE (OE) and its complete parallel control Lenti-SFFV-CoGFP-IRES-PURO-WPRE (NC) were synthesized by PPL and use to established stable expression PDZK1 (Huh7-OE) and control (Huh7-NC) cells.

Cell viability assay

Cell viability was assessed by employing the Cell Counting Kit-8 (CCK8) (MA0218,MeilunBio) in accordance with the guidelines provided by the manufacturer. The cells were seeded into 96-well plates at a density ranging from 2 to 3×10^3 cells per well. Following a duration of 48 h, the cell culture medium was substituted with fresh DMEM supplemented with 10% CCK8 solutions, and the plates were reintroduced into a 37 °C incubator for a period of 3 h. The absorbance at 450 nm was then quantified using a spectrophotometer.

Cytotoxicity assay

Cell cytotoxicity was assessed by CCK8. The cells were seeded into 96-well plates at a density of 2×10^5 cells per well and subsequently subjected to Oxaliplatin (OXA; Sanofi) treatment (0, 10, 20, 30, 40, 50, 60μmol/L). Following a duration of 48 h, the cell culture medium was substituted with fresh DMEM supplemented with 10% CCK8 solutions, and the plates were reintroduced into a 37 °C incubator for a period of 3 h. The absorbance at 450 nm was then quantified using a spectrophotometer.

RNA extraction and quantitative real-time PCR (qPCR)

Cell RNA was extracted using TransZol Up (ET111-01-V2, TransGen Biotech) following the manufacturer's instructions. The RNA was then reverse transcribed into cDNA using the TransScript® Uni All-in-One First-Strand cDNA Synthesis SuperMix for qPCR (One-Step gDNA Removal) (AU341-02, TransGen Biotech). mRNA expression was assessed by qPCR using MagicSYBR Mixture (CW3008M, CWBIO) on the LightCycler®96 (Roche). Actin was used as the internal control for PCR amplification to measure the expression of target genes. The primers used are listed in Table S1.

Western blot

Protein was extracted from cell with RIPA lysis buffer (AR0102, Boster Biological Technology) with freshly added protease and phosphatase inhibitor cocktail(AR1192, Boster Biological Technology). Protein concentrations were determined with a Bicin-choninic Acid Protein Assay Kit (CW0014S, CWBIO). The equal amount of protein samples were resolved by SDS-PAGE and transferred onto PVDF membranes. After blocking for 3 h at room temperature in 10% skim milk, the membranes were incubated at 4 °C overnight with primary antibodies (Table S2). The membranes were then washed three times and incubated for 2 h at room temperature with a respective IgG-HRP labeled second antibody(CWBIO Cat#CW0103S,1:2000 dilution, RRID: AB_3251479). Antigens were revealed using a chemiluminescence assay (BL520A, Biosharp) on a Chemiluminescent Image System (SinSage).

Immunohistochemistry (IHC)

The clinical samples was sectioned by the Pathology Laboratory at the First Affiliated Hospital of Shanxi Medical University. Subsequently, the slides were stained using PDZK1(HUABIO Cat#ER1914-96, RRID: AB_3668634, MRP2(HUABIO Cat#ET1704-47, RRID: AB_3070494) antibody. The imaging was performed using the PANNORAMIC scan II (3DHISTECH). Immunohistochemical staining was evaluated using the following scoring system: Staining intensity was scored as 0–8. The histochemical scoring of pathological slides was completed by 2 experienced pathologists from First Affiliated Hospital of Shanxi Medical University who were blinded to the clinical data. Areas of necrosis or artifact were excluded from the analysis.

Co–immunoprecipitation (Co–IP)

In IP assay, HEK-293T cells were transfected and seeded in 100 mm Cell Culture Dishes. After 48 h, cells were lysed with IP lysis buffer (26149, Thermo Fisher Scientific). The samples were moved to a centrifuge tube and inverted repeatedly for 1 h at 4 °C. Following centrifugation at 15,000 rpm for 15 min at 4 °C. After the addition of FLAG Beads (Sigma-Aldrich Cat# M8823, RRID: AB_2637089), incubation was continued for an additional 3 h at 4 °C. Following centrifugation at 6,000 rpm for 3 min. The beads were then washed four times with Wash Buffer (26149, Thermo Fisher Scientific) before being boiled in SDS loading buffer. In CO-IP study, after washing in PBS, HepG2 cells were lysed in ice-cold lysis buffer. Then, 10 μg of PDZK1 antibody (Proteintech Cat# 10507-2-AP, RRID: AB_2299495) or appropriate control Rabbit IgG (Beyotime Cat# A7016, RRID: AB_2905533) was immobilized with Pierce Co-Immunoprecipitation (Co-IP) Kit(26149, Thermo Fisher Scientific).After that, cell lysates was precipitated and eluted with Co-IP Kit. Then, the immunoprecipitates were boiled in SDS-PAGE loading buffer for subsequent Western blotting.

Immunofluorescence analysis

In this study, HepG2 and HEK-293T cells were seeded and treated in 24-well plates with cell climbing slices. The cells in the cell climbing slices were fixed using a 4% polyformaldehyde solution, and Triton X-100 (T8200, Solarbio) was employed to disrupt the cell membrane. Subsequently, the cells were blocked for 30 min using normal goat serum (AR0009,Boster Biological Technology) and then incubated overnight at 4 with primary antibodies: anti-PDZK1 antibody (Santa Cruz Biotechnology Cat# sc-390964, RRID: AB_3065082,1:50 dilution), anti-MRP2 antibody (HUABIO Cat#ET1704-47, RRID: AB_3070494,1:50 dilution), anti-HA antibody(ABclonal Cat# AE008, RRID: AB_2770404,1:50 dilution) and anti-FLAG antibody(HUABIO Cat#0912-1, RRID: AB_3068715,1:250 dilution). After washing the cells with PBS-T three times, the cells were incubated with FITC Conjugated Goat anti-Rabbit IgG polyclonal Antibody (HUABIO Cat# HA1004, RRID: AB_3668636,1;50 dilution) and TRITC Conjugated Goat Anti-Mouse IgG H&L polyclonal Antibody (HUABIO Cat# HA1017, RRID: AB_3668635,1:50dilution) for 1 h at room temperature. Finally, DAPI (AR1176, Boster Biological Technology) and anti-quenching sealant (AR1109, Boster Biological Technology) was applied to the slides, and confocal laser microscope imaging was used to capture the images.

Wound healing assay

Briefly, cells were seeded in 6-well plates, reaching 80% confluence and then carefully scratched with a sterile 200 μL pipette tip. After that, these cells were incubated in medium containing OXA at a concentration of 30 μM. Finally, the wounds were monitored and photographed by a light microscope (Guangzhou MSHOT) at 0, 24 ,48 h. The result of wound-healing was analyzed using ImageJ (RRID: SCR_003070).

Transwell assay

Transwell chambers (34264, Corning) were used for cell Migration assays. Transwell chambers (34264, Corning) precoated with Basement Membrane Matrix (HY-K6002, MedChemExpress) were used for cell invasion assays. First, 500 μL of medium with 20% FBS was added to the lower chamber, and cells with indicated treatments in 200 μL medium containing OXA at a concentration of 30 μM and 0% FBS were added to the upper chamber. After 24 h of incubation at 37 °C, the cells on the lower surface of the chamber membrane were fixed in 4%

paraformaldehyde (DF0135, Leagene), stained with 0.1% crystal violet (C8470, Solarbio) and counted under a microscope.

Animal experiments

All animal experiments were conducted in strict adherence to the "Guide for the Care and Use of Laboratory Animals" issued by the National Institutes of Health and were granted approval by the Animal Ethics Committee of Shanxi Medical University (Authorization Number: DWYJ-2023-016). BALB/C nude mice were accommodated in an animal facility featuring a 12-hour light-dark cycle, with a controlled temperature maintained at 20–22 °C and a humidity level kept between 40% and 70%. For the establishment of subcutaneous tumor models, the nude mice were randomly assigned to two groups: a control group ($n = 5$) and an overexpression group ($n = 5$). Subsequently, five million Huh7-NC and Huh7-OE cells were injected into 5-week-old male BALB/C nude mice(RRID: IMSR_APB:4790), respectively. Drug administration commenced when the tumor tissues had reached a volume of 50 mm³ after a period of 14 days. At this juncture, the mice within each group were further randomized to receive oxaliplatin (administered intraperitoneally at a dosage of 7.5 mg/kg every 2 days). The tumor size and body weight of the mice were meticulously recorded every 2–3 days. After a duration of 30 days, the mice were euthanized via cervical dislocation under isoflurane anesthesia for the purpose of tumor collection. The weight and volume of the excised tumors were then accurately recorded. All experiments were performed in accordance with relevant guidelines and regulations.

Equipment and settings

Figure 1A–E, G, H, and I were generated using GraphPad Prism. One part of F was captured with professional equipment from the Department of CT Imaging, The First Hospital of Shanxi Medical University. The remaining part of F was acquired using the PANNORAMIC Scan II (3D HISTEC) and analyzed with CaseViewer software. Figure 2A, D, and G were developed using a Chemiluminescent Imaging System with an exposure time of approximately 150–200 ms. C, F, and I were taken with a Guangzhou Mingmei optical microscope, while the rest were plotted using GraphPad Prism. Figure 3A–C were generated through database analysis using R 4. 0. D and F were acquired in the same manner as A of Fig. 2E was captured using a fluorescence microscope with a magnification of 10X. G was obtained with a fluorescence confocal microscope at 63X magnification. Figure 4A, D, and G were captured in the same manner as A of Fig. 2C, F, I, and J were processed similarly to C of Fig. 2. The sharpening of J was completed using Microsoft Office software. Figure 5A was captured in the same way as F of Fig. 1, while the remaining panels were created using GraphPad Prism. All figures were compiled using Adobe Illustrator 2025 and exported at 300 dpi resolution after adjustments in Photoshop.

Statistical analysis

The data were analyzed using two-tailed unpaired Student's t-test with SPSS (RRID: SCR_002865) (version 26, IBM Corp.). The image were made by GraphPad Prism (RRID: SCR_002798) (version 9.0, GraphPad Software Inc.). The counting of cells is done by Image J. Each experiment included a minimum of three independent samples. A p value less than 0.05 was considered statistically significant. (ns = not significant, $*P < 0.05$, $**P < 0.01$, $***P < 0.001$).

All methods were carried out in accordance with relevant guidelines and regulations.

Results

PDZK1 as a novel oxaliplatin chemosensitivity biomarker for hepatocellular carcinoma

To identify a potential biomarker for OXA chemosensitivity in hepatocellular carcinoma (HCC), we explored the RNA-seq database from GSE51951, TCGA-LIHC and the Chinese Liver Cancer Atlas (CLCA) project. The process of screening differentially expressed genes (DEGs) through transcriptome analysis is shown in Fig. 1A. The cut-off value was defined as ｜ fold change ｜ > 1.5 and p value < 0.001. The results showed that 62 DEGs (including 40 up-regulated and 22 down-regulated genes) were identified in the OXA-resistant MHCC97H group and control MHCC97H group of GSE51951. In addition, 5427 DEGs (including 2419 up-regulated and 3008 down-regulated genes) were screened from 47 cases of HCC and paired adjacent tissues in TCGA-LIHC. The Venny plot showed that 8 co-existing DEGs (including 4 up-regulated genes: *CLDN15*, *PDGFA*, *PDZK1*, *TPTE2P1* and 4 down-regulated genes: *CETP*, *S1PR4*, *SPOCK3*, *VSIG4*) were identified in both cohorts. Further analyze the relationship between the expression levels of the above 8 genes and the relapse-free survival (RFS) of CLCA database (Fig. 1B-D). The results showed that in the CLCA database, the Kaplan-Meier curves revealed that high-PDZK1 HCC group had a shorter RFS time, while the other seven genes were not correlated with RFS (Fig. S1) .

In order to further validate the screening results of the public database, we collected 39 HCC patients tissue treated with OXA chemotherapy at the First Hospital of Shanxi Medical University, and performed PDZK1 immunohistochemical staining (IHC) on samples that recurrent ($n = 18$) and non-recurrent ($n = 21$) within one year (Fig. 1E). Detailed clinical data is listed in Table 1. The results showed that the expression of PDZK1 in the HCC recurrence group based on CT diagnosis was higher than that in the non-recurrence group (Fig. 1F-H), and patients in the PDZK1 high expression group had poorer RFS (Fig. 1I). The above results indicated that PDZK1 acted a potential biomarker for promoting HCC patients recurrence by affecting the sensitivity to OXA-chemotherapy.

PDZK1 suppresses OXA chemosensitivity of hepatocellular carcinoma

To explore the effect of PDZK1 on chemotherapy sensitivity of HCC cells, we first established a HepG2 cell model with transient overexpression of PDZK1. The results showed that the protein level of PDZK1 significantly increased after transient transfection (Fig. 2A). The cell function experiment aims to detect the changes in cell
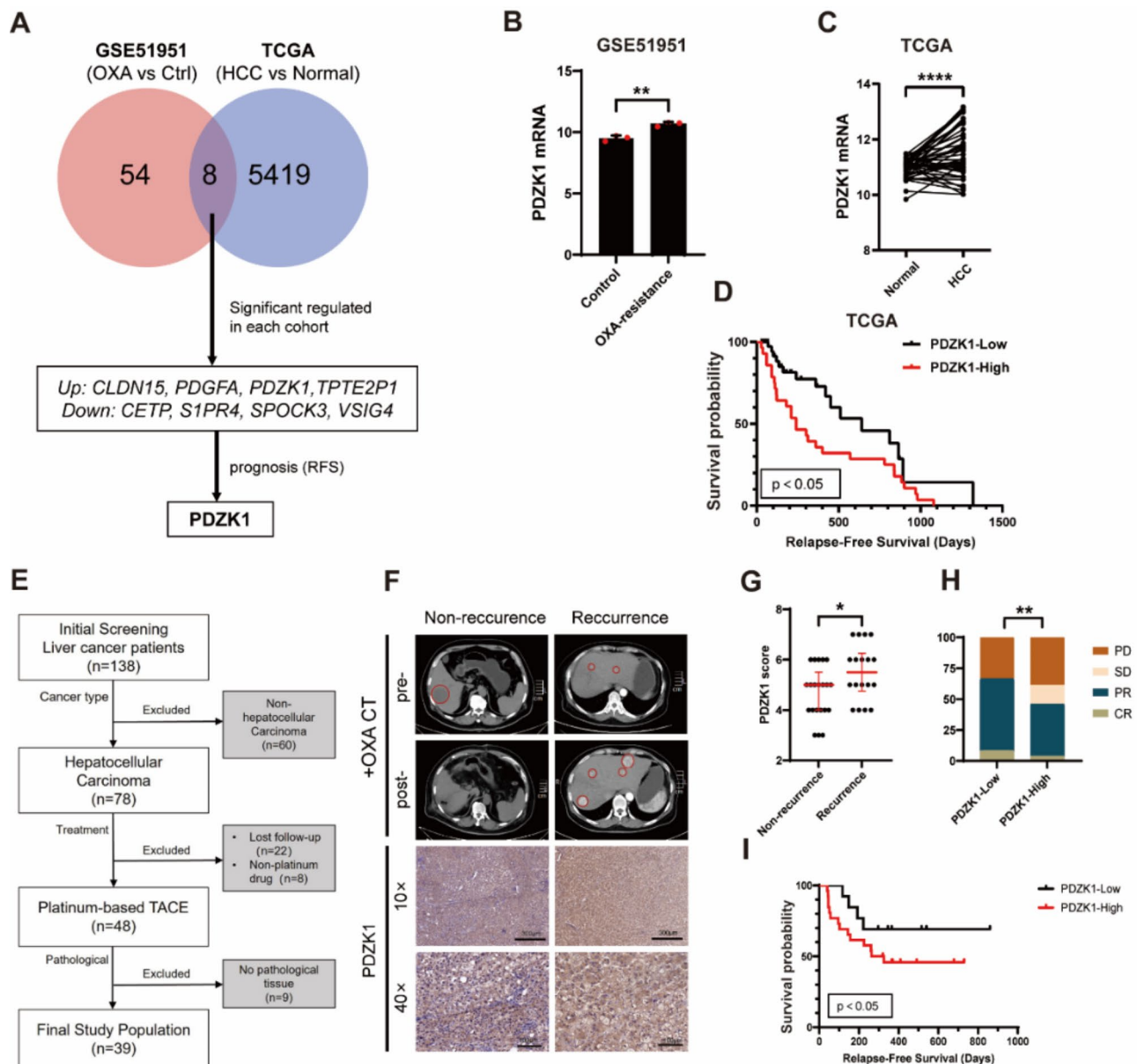
Fig. 1. High expression of PDZK1 is associated with recurrence of HCC treated with oxaliplatin. **A** The flowchart of gene screening. The left side of the Venny diagram represents the differentially expressed genes (DEGs) of oxaliplatin-resistant MHCC97H ($n = 3$) or control MHCC97H ($n = 3$) in GSE51951 database, while the right side represents the DEGs of the HCC group ($n = 47$) and its paired normal ($n = 47$) in TCGA-LIHC database. Both databases were screened based on ∣ fold change ∣ ≥ 1.5 and $p < 0.001$, resulting in 8 DEGs. Then, the relationship between the expression of the 8 genes mentioned above and RFS in HCC patients of CLCA database was analyzed, and PDZK1 was obtained. **B** PDZK1 expression in oxaliplatin-resistant ($n = 3$) and control MHCC97H HCC cell in GSE51941 database. Unpaired t-test, $**p < 0.01$. **C** PDZK1 expression in HCC group ($n = 47$) and its paired normal ($n = 47$) in TCGA-LIHC database. Paired t-test, $**** p < 0.0001$. **D** Kaplan-Meier plot for relapse-free survival (RFS) based on PDZK1 mRNA expression of HCC patients after treatment in CLCA database ($p < 0.05$, log-rank test). **E** The screening process for clinical cases of HCC treated with oxaliplatin included in this study. **F** Abdominal CT images and immunohistochemical schematic of PDZK1 protein expression for HCC non-recurrence and recurrence after OXA treatment. **G** Statistical chart of PDZK1 immunohistochemical scores for non recurrent and recurrent OXA-treated HCC. Unpaired t-test, $*p < 0.05$. **H** Distribution of different treatment outcomes for non-recurrent and recurrent OXA-treated HCC. Fisher's exact test, $**p < 0.01$. **I** The relationship between PDZK1 protein expression and relapse-free survival (RFS) of OXA-treated HCC.
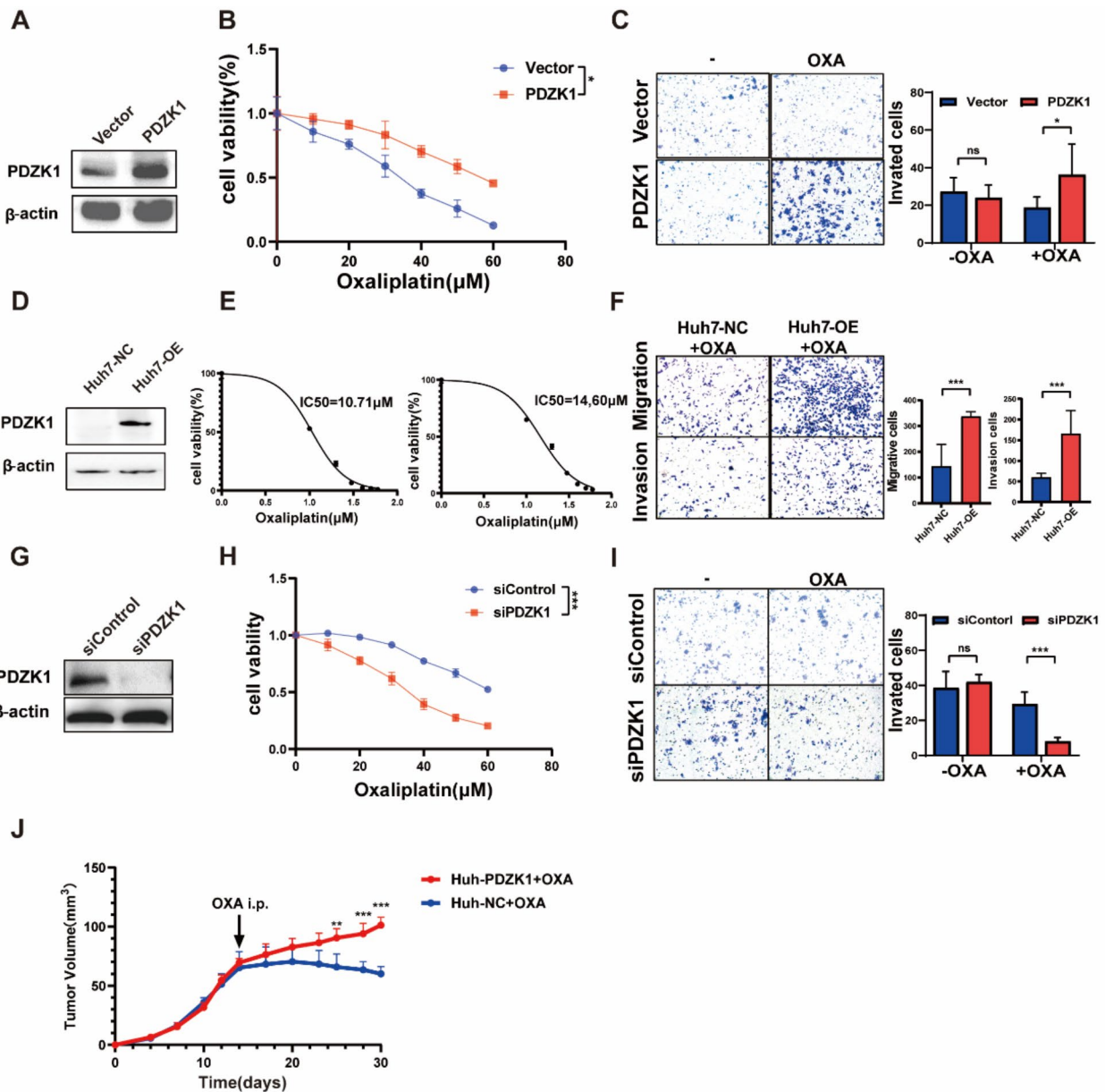
Fig. 2. PDZK1 suppresses OXA chemosensitivity of hepatocellular carcinoma. **A** Western Blot (cropped images) analysis of PDZK1 expression in PDZK1-overexpressed and control HepG2 cells. **B** Cell viability of OXA treated PDZK1-overexpressed and control HepG2 cells. Repeated measurement ANOVA, * $p < 0.05$. **C** Transwell invasion assay of OXA treated PDZK1-overexpressed and control HepG2 cells. Unpaired t-test, ns represents $p > 0.05$, * $p < 0.05$. **D** Western Blot (cropped images) analysis of PDZK1 expression of PDZK1 stable overexpression (Huh7-PDZK1-OE) and control (Huh7-PDZK1-NC) cells. **E** Cell viability and IC50 value of Huh7-PDZK1-NC (left) and Huh7-PDZK1-OE (right) cells treated with OXA concentration gradient for 48 h. **F** Transwell migration and invasion assay of OXA-treated Huh7-PDZK1-NC and Huh7-PDZK1-OE cells. Unpaired t-test, *** $p < 0.001$. **G** Western Blot (cropped images) analysis of PDZK1 expression in siPDZK1 and control HepG2 cells. **H** Cell viability of OXA treated siPDZK1 and control cells. Repeated measurement ANOVA, *** $p < 0.001$. **I** Transwell invasion assay of OXA treated siPDZK1 and control cells. Unpaired t-test, ns represents $p > 0.05$, *** $p < 0.001$. **J** Subcutaneous transplantation tumor model detection of Huh7-NC and Huh7-PDZK1 chemotherapy sensitivity to OXA. Two-way ANOVA, * $p < 0.05$, ** $p < 0.01$, *** $p < 0.001$.

viability, invasion, and migration ability of PDZK1 after treatment with or without OXA. The results showed that after treatment with 30 μM OXA for 48 h, the cell viability (Fig. 2B), cell invasion (Fig. 2C), and cell migration (Fig. S3A-C) of overexpressing PDZK1 group were significantly stronger compared to the control group. Consistent with the above results, Huh7 cells stably overexpressing PDZK1 enhanced cell viability, invasion and migration ability after OXA treatment (Fig. 2D-F). Subsequently, we established a PDZK1 knockdown cell model using small interfering RNA (Fig. 2G). The results of the functional experiment indicated that after treatment with
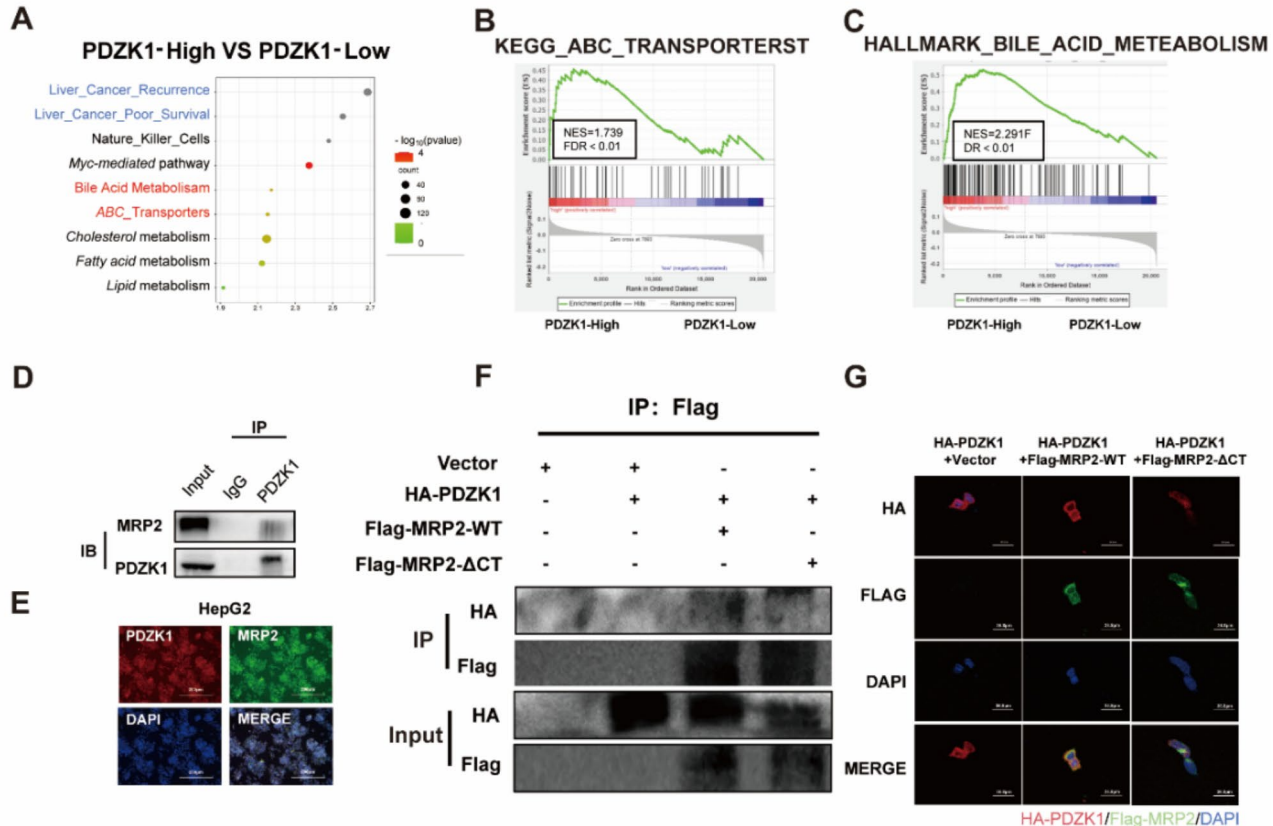
Fig. 3. PDZK1 interacts with MRP2. **A** Divide the PDZK1 expression of liver cancer patients in the TCGA-LIHC database into PDZK1 high expression and PDZK1 low expression groups according to the mean. Screening MRP2 mediated pathway (*Bile_Acid_Metabolism*, *ABC_Transporters*) as PDZK1 differential pathway according to GSEA analysis. **B-C** GSEA analysis of *KEGG_ABC_TRANSPORTERST* (B) and *HALLMARK_BILE_ACID_METABOLISM* (C) Pathway in PDZK1-high group and PDZK1-low expression group. FDR < 0.20 is considered statistically significant. **D** The interaction between PDZK1 and MRP2 was detected by Co-IP in HepG2 cells (cropped images). **E** The co-localization between PDZK1 and MRP2 was verified by immunofluorescence in HepG2 cells (cropped images). **G** Detecting the interaction by Co-IP assay (**F**) and co-localization (**G**) by of immunofluorescence transient transfection HA-PDZK1 and Flag-MRP2-WT/Flag-MRP2-ΔCT in 293T cells.

30μM oxaliplatin for 48 h, the expression of PDZK1 is reduced, and the cell viability (Fig. 2H), invasion (Fig. 2I), and migration (Fig. S3D-F) ability of the group were significantly reduced. Two groups of cells, Huh7-NC and Huh7-PDZK1, were implanted subcutaneously into nude mice at a cell count of 5×10^6 per mouse. On the 14th day after implantation, OXA was intraperitoneally injected, and tumor volume was measured every 2–3 days for a total of 30 days of observation. The results showed that compared to the Huh7 NC group, the Huh7-PDZK1 group had a larger tumor volume after OXA treatment (Fig. 2J). In total, we found that PDZK1 inhibited the sensitivity of OXA chemotherapy.

PDZK1 inhibits MRP2-mediated OXA chemosensitivity through interaction with MRP2

In order to explore the potential mechanism of PDZK1 inhibiting OXA chemosensitivity, we used a RNA-seq database to divide HCC patients into two groups: PDZK1-low expression group and PDZK1-high expression group. Differential pathway enrichment analysis showed that in the PDZK1-high expression group, the top ten significantly activated signaling pathways are *Liver_Cancer_Recurrence*, *Liver_Cancer_Poor_Survival*, *Nature_Killer_T_Cells*, *Myc-mediated pathway*, *Bile_Acid_Metabolisam*, *ABC_Transporters*, *Cholesterol metabolism*, *Fatty acid metabolism and Lipid metabolism* (Fig. 3A–C). MRP2 was a gene related to bile acid metabolism and ABC transporter pathway, so MRP2-related signaling pathway is significantly activated in the PDZK1-high expression group. Endogenous Co-IP assay and immunofluorescence (IF) staining were performed on HepG2, and the results showed that PDZK1 interacted with MRP2 (Fig. 3D) and PDZK1 and MRP2 co-localized in the cytoplasm in HepG2 (Fig. 3E). PDZ proteins, including PDZK1, typically interact with the carboxyl terminus of their interacting proteins[12–14]. Therefore, we constructed HA-PDZK1, Flag-MRP2-WT, and Flag-MRP2- ΔCT to validate the interaction sites between PDZK1 and MRP2. The results showed that the interaction between
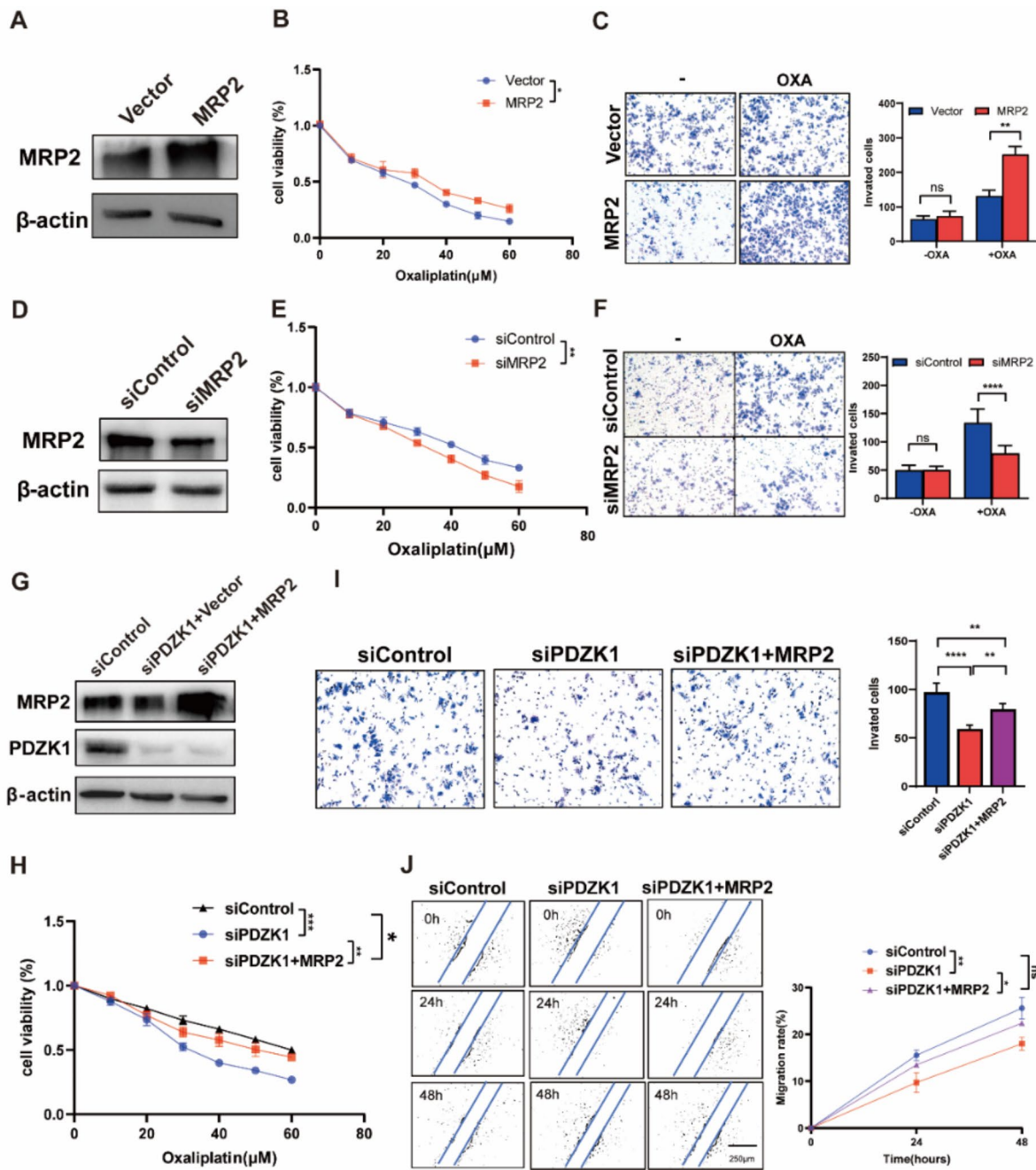
Fig. 4. PDZK1 inhibits OXA chemosensitivity through MRP2. **A** MRP2 protein expression levels as shown by Western Blot (cropped images) in transient MRP2 overexpression HepG2 cells. **B** Cell viability of OXA treated MRP2-overexpressed and control HepG2 cells. Repeated measurement ANOVA, * $p < 0.05$. **C** Transwell invasion assay of OXA treated MRP2-overexpressed and control HepG2 cells. Unpaired t-test, ns represents $p>0.05$, ** $p < 0.01$. **D** MRP2 protein expression levels as shown by Western Blot (cropped images) in siMRP2 and control HepG2 cells. **E** Cell viability of OXA treated siMRP2 and control HepG2 cells. Repeated measurement ANOVA, ** $p < 0.01$. **F** Transwell invasion assay of OXA treated siMRP2 and control HepG2 cells. Unpaired t-test, ns represents $p>0.05$, **** $p < 0.0001$. **G** Western Blot (cropped images) analysis of PDZK1 and MRP2 expression in co-transfection of PDZK1 small interfering RNA and MRP2 plasmid and control HepG2 cells. **H** Cell viability were used to detected cell function of sicontrol, siPDZK1 and siPDZK1 + MRP2. Post-hoc test with repeated measurement ANOVA., * $p < 0.05$, ** $p < 0.01$, *** $p < 0.001$. **I** Transwell invasion assay were used to detected cell function of sicontrol, siPDZK1 and siPDZK1 + MRP2. Post-hoc test with one-way ANOVA, ns represents $p>0.05$, **** $p < 0.0001$. **J** Wound healing assay were used to detected cell function of sicontrol, siPDZK1 and siPDZK1 + MRP2. Post-hoc test with repeated measurement ANOVA, ns represents $p>0.05$, * $p < 0.05$, ** $p < 0.01$.
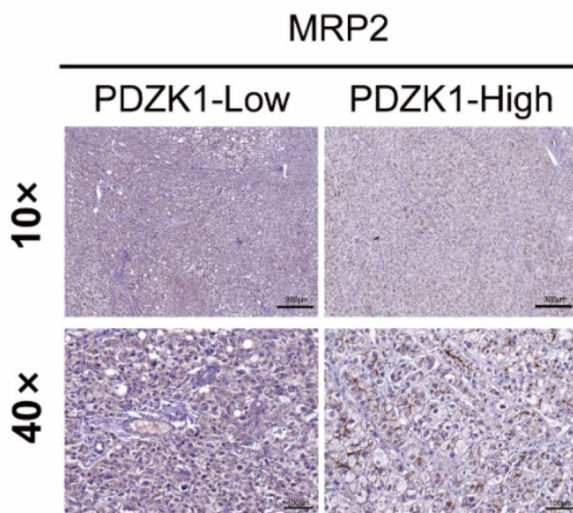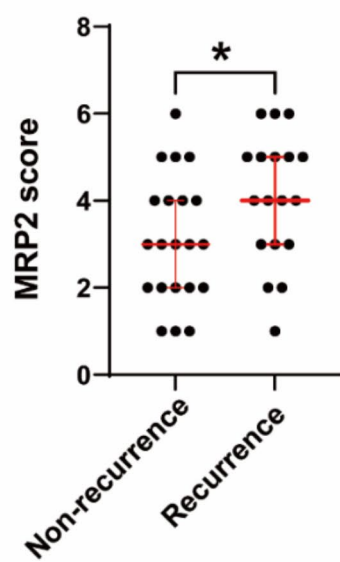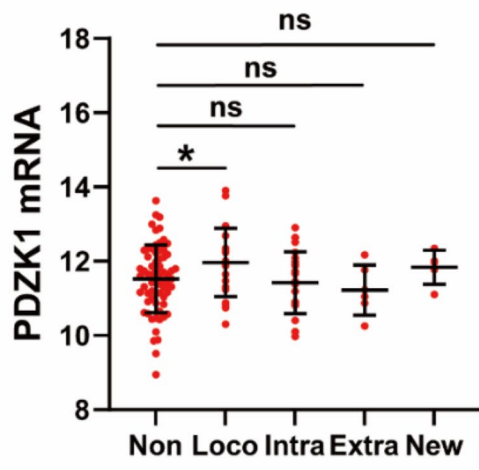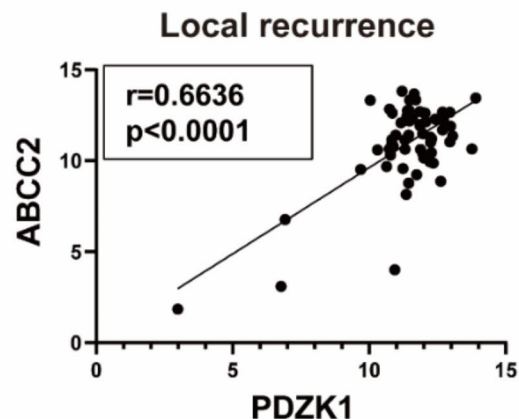
Fig. 5. Low expression of PDZK1 is positively correlated with MRP2-mediated OXA chemotherapy response in HCC patients. **A-B** HCC clinical patients were divided into PDZK1 high expression group and PDZK1 low expression group according to the PDZK1 immunohistochemical score, and the MRP2 protein expression between the two groups was compared. Mann-Whitney test. *$p < 0.05$. **C** In the TCGA-LIHC database, HCC patients were divided into non-recurrent, locally recurrent, intrahepatic recurrent, extrahepatic recurrent, and newly HCC groups based on clinical data. Unpaired *t*-test, ns represents $p > 0.05$, * $p < 0.05$. **D** The expression of PDZK1 and MRP2 was significantly correlated in HCC patients with local recurrence. Pearson correlation analysis, $r = 0.6636$, $p < 0.001$.

MPR2 and PDZK1 was weakened after the carboxyl terminus was mutated (Fig. 3F), and co-localization in the cytoplasm was also weakened (Fig. 3G). Overall, PDZK1 interacts with MRP2 through the carboxyl terminus of MRP2 in HCC cells.

MRP2 is widely studied as a multidrug resistance protein, but its effect on oxaliplatin sensitivity in HCC had not been reported. Therefore, we first established a HCC cell model of overexpression and knockdown of MRP2 (Fig. 4A and D). The results of cell function experiments showed that overexpression of MRP2 enhanced the cell viability, invasion, and migration ability of HCC cells (Figs. 4B, C, S4A). After reducing MRP2, cell viability, invasion, and migration decreased (Figs. 4D–F, S4B). To further validate the effect of PDZK1 on OXA chemosensitivity through MRP2, we overexpressed MRP2 on the basis of siPDZK1. The protein expression of PDZK1 and MRP2 was detected (Fig. 4G). The results showed that compared with the control group, the cell viability of the siPDZK1 group significantly decreased, while cell viability was restored after overexpression

of MRP2 (Fig. 4H). Similarly, we found that overexpression of MRP2 could restore the ability to reduce cell invasion and migration cased by knocking down PDZK1 (Fig. 4I, J).

Low expression of PDZK1 is positively correlated with MRP2-mediated OXA chemotherapy response in HCC patients

We further validated the relationship between PDZK1 and MRP2 at the clinical level. Immunohistochemical results showed that MRP2 expression was elevated in the PDZK1 high expression group and OXA non-response group (Fig. 5A, B). HCC patients with high PDZK1 expression were more likely to experience in local recurrence (Fig. 5C), and PDZK1 and MRP2 expression were positively correlated in HCC recurrence specimens (Fig. 5D). The above results further demonstrate the close positive correlation between high expression of PDZK1 and MRP2 in clinical practice.

Discussion

Liver cancer was the fourth most common and second most lethal cancer in China. Among them, hepatocellular carcinoma (HCC) accounted for the highest proportion of primary liver cancer, at 75–85%[1,4,27]. oxaliplatin (OXA)-based on TACE or HAIC has significant therapeutic effects on patients in advanced HCC[2,4,10]. Although there was a possibility of acquired resistance after OXA chemotherapy, it was particularly important to understand the underlying mechanisms of initial sensitivity to OXA in order to distinguish between patients who responded to OXA or not. Our study was based on differential gene screening for OXA-based chemotherapy response, and functionally found that high expression of PDZK1 has an inhibitory effect on OXA chemotherapy sensitivity. Further investigation revealed that the MRP2 mediated signaling pathway was a critical signaling pathway for PDZK1 to inhibit sensitivity to OXA chemotherapy. MRP2 interacted with PDZK1 in HCC cells and co-localized in the cytoplasm. Finally, we validated that HCC patients with low PDZK1 expression were more sensitive to oxaliplatin chemotherapy.

As a scaffold protein, PDZ protein can interact with various transmembrane proteins and key signaling pathway molecules, thereby regulating the function of interacting proteins[12–15,19–21,28]. The relationship between PDZK1 and cancer has been extensively studied[12–15]. PDZK1 inhibited the phosphorylation of PTEN and thus suppressed the growth of gastric cancer[12]. In addition, PDZK1 confers sensitivity to sunitinib in clear cell renal cell carcinoma by inhibiting the phosphorylation of PDGFR[14]. Also, PDZK1 suppressed triple-negative breast cancer growth and sensitivity to erlotinib by regulating EGFR[13]. In liver cancer, PDZK1 is considered an oncogene[16–18]. Gao et al. reported that PDZK1 was significantly higher in HCC specimens than in adjacent specimens[17]. PDZK1 promoted the malignant phenotype of HCC cells by activating the PI3K/AKT signaling pathway[17,18]. Based on bioinformatics analysis, Chen et al. found that *pdzk1* may act as a oncogene promoting HBV infection related HCC, and is closely related to fatty acid metabolism and Treg-induced immunosuppression[18].

During our gene screening process, in addition to *PDZK1*, there were three up-regulated genes (*CLDN15*, *PDGFA*, *TPTE2P1*) and four down-regulated genes (*CETP*, *S1PR4*, *SPOCK3*, *VSIG4*) in the OXA-resistant (GSE51951) and HCC groups (TCGA-LIHC). CLDN15 (claudin-15) is a member of the claudin family and functions as a tight junction protein. CLDN15 was up-regulated in lung adenocarcinoma[29] and malignant pleural mesothelioma[29–31], and acted as a potential tumor suppressor gene in colorectal cancer[32,33], but its role in HCC has not been reported. PDGFA also known as a platelet-derived growth factor receptor alpha, which was up-regulated in HCC[34,35]. Chen et al. reported that HCC induces the extracellular matrix (ECM) remodeling by activating the TGFβ-PDGFA pathway and recruiting cancer-associated fibroblasts (CAFs)[36]. The long noncoding RNA (lncRNA) transmembrane phosphoinositide 3-phosphatase and tensin homolog 2 pseudogene 1 (TPTE2P1) played roles in tumor progression, including colorectal cancer[37], thyroid carcinoma[38], gallbladder cancer[39] and hepatocellular carcinoma (HCC)[40]. TPTE2P1 was overexpressed in HCC tissues and cell lines, and is associated with tumor size, distant metastasis, differentiation degree, and TNM staging. It was confirmed that overexpression of TPTE2P1 promotes the migration and invasion of HCC cells, and increases the protein levels of E-cadherin, Vimentin, and N-cadherin. Therefore, lncRNA TPTE2P1 may serve as an early biomarker and therapeutic target for HCC metastasis[40]. CETP (Cholesteryl ester transfer protein) regulated the reverse cholesterol transport and was associated with microvascular invasion, tertiary lymphoid structure (TLS), and necroptosis in HCC[41–43]. S1PR4 (Sphingosine 1-phosphate receptor 4) is a receptor for the lysosphingolipid sphingosine 1-phosphate (S1P). Yoshida and Matsushima-Nishiwaki et al. reported that S1PR4 antagonist has no significant effect on HCC occurrence[44,45]. SPOCK3, also called (Testican-3,TICN3), was widely known as a tumor progression and prognostic biomarker for prostate cancer[46], and it was considered to predict chemotherapy sensitivity in colorectal cancer. However, its role in liver cancer has not been studied. V-set and immunoglobulin domain-containing protein 4 (VSIG4) is a negative regulator of T cell activation. Zhu et al.[47] reported that low expression level of VSIG4 was associated with poor prognosis of HBV-related HCC.

Multidrug resistance protein 2 (MRP2, also called ATP-binding cassette sub-family C member 2, ABCC2) is an ATP binding cassette (ABC) transporter protein, mainly expressed on the basement membrane of human liver cells, and also on the apical membrane of polar cells such as epithelial cells in the renal proximal tubules[48–50]. MRP2 inhibit tumor cell sensitivity to oxaliplatin by exocytosis[51]. In addition, as a key receptor for bile acid metabolism, MRP2 promotes the malignant progression of liver cancer by activating inflammasomes[50]. Although protein-protein interactions between PDZK1 and MRP2 have been reported[52–54], it is still unknown whether PDZK1 affects OXA related chemotherapy sensitivity through MRP2 interactions. The class II PDZ domain-binding motif (-X-Psi-X-Psi, Psi represents any hydrophobic amino acid) at the carboxy terminus of MRP2 (which the last four amino acid is -STKF) is essential for targeting PDZ protein. Therefore, in our study, we constructed two plasmids, MRP2 wild type and MRP2 mutant type (delAA1542-1545) with flag tag to verified their interaction with PDZK1. The results showed that compared with the wild group, the interaction and cell co-localization between MRP2 and PDZK1 in the mutant group were significantly weakened. After knocking

down PDZK1 and overexpressing MRP2, siPDZK1 induced the chemotherapy sensitivity of OXA was inhibited. In this study, we confirmed that PDZK1 affected the OXA chemosensitivity of HCC by directly influencing the MRP2 mediated signaling pathway.

The limitation of this study is that, based on the clinical treatment plan of oxaliplatin and combination therapy, it is unknown whether PDZK1 has an effect on other drugs. Secondly, simple TACE and HAIC can also lead to drug resistance. Therefore, future research can expand the clinical sample library and compare and validate multiple treatment options.

Conclusion

In summary, we revealed that high expression of PDZK1 is highly correlated with poor prognosis and non-response to OXA chemotherapy in HCC patients. The possible mechanism was that PDZK1 directly regulated MRP2-mediated OXA chemotherapy insensitivity.

Data availability

Data is provided within the manuscript or supplementary information files.

References

1. Sung, H. et al. Global Cancer statistics 2020: GLOBOCAN estimates of incidence and mortality worldwide for 36 cancers in 185 countries. *CA Cancer J. Clin.* **71**, 209–249 (2021).
2. Reig, M. et al. BCLC strategy for prognosis prediction and treatment recommendation: the 2022 update. *J. Hepatol.* **76**, 681–693 (2022).
3. Sidali, S., Trepo, E., Sutter, O. & Nault, J. C. New concepts in the treatment of hepatocellular carcinoma. *United Eur. Gastroenterol. J.* **10**, 765–774 (2022).
4. Xie, D. Y. et al. A review of 2022 Chinese clinical guidelines on the management of hepatocellular carcinoma: updates and insights. *Hepatobiliary Surg. Nutr.* **12**, 216–228 (2023).
5. Tavakoli Pirzaman, A. et al. The role of MicroRNAs in regulating Cancer cell response to Oxaliplatin-Containing regimens. *Technol. Cancer Res. Treat.* **22**, 15330338231206003 (2023).
6. Shi, Y. et al. PRMT3-mediated arginine methylation of IGF2BP1 promotes oxaliplatin resistance in liver cancer. *Nat. Commun.* **14**, 1932 (2023).
7. Zhong, S., Wang, Z., Yang, J., Jiang, D. & Wang, K. Ferroptosis-related oxaliplatin resistance in multiple cancers: potential roles and therapeutic implications. *Heliyon* **10**, e37613 (2024).
8. Shen, J. H. et al. HSF1/AMPKalpha2 mediated alteration of metabolic phenotypes confers increased oxaliplatin resistance in HCC cells. *Am. J. Cancer Res.* **9**, 2349–2363 (2019).
9. Cao, H., Yang, M., Yang, Y., Fang, J. & Cui, Y. PBK/TOPK promotes chemoresistance to oxaliplatin in hepatocellular carcinoma cells by regulating PTEN. *Acta Biochim. Biophys. Sin (Shanghai)* **53**, 584–592 (2021).
10. Zhang, F. et al. Oxaliplatin-Resistant hepatocellular carcinoma drives immune evasion through PD-L1 Up-Regulation and PMN-Singular recruitment. *Cell. Mol. Gastroenterol. Hepatol.* **15**, 573–591 (2023).
11. Weng, J. et al. Periplocin improves the sensitivity of oxaliplatin-resistant hepatocellular carcinoma cells by inhibiting M2 macrophage polarization. *Biomol. Biomed.* (2024).
12. Zhao, C. et al. Loss of PDZK1 expression activates PI3K/AKT signaling via PTEN phosphorylation in gastric cancer. *Cancer Lett.* **453**, 107–121 (2019).
13. Ma, Y. et al. PDZK1 suppresses TNBC development and sensitizes TNBC cells to erlotinib via the EGFR pathway. *Cell. Death Dis.* **15**, 199–203 (2024).
14. Wang, H. et al. PDZK1 confers sensitivity to Sunitinib in clear cell renal cell carcinoma by suppressing the PDGFR-beta pathway. *Br. J. Cancer* **131**, 347–360 (2024).
15. Ren, X., Deng, D., Xiang, S. & Feng, J. Promoter hypomethylated PDZK1 acts as a tumorigenic gene in glioma by interacting with AKT1. *Aging (Albany NY)* **16**, 7174–7187 (2024).
16. Guo, L. et al. Mechanism of PDZK1 in hepatocellular carcinoma complicated with hyperuricemia. *J. Oncol.* **2022**, 1403454 (2022).
17. Gao, H. et al. miR-101-3p-mediated role of PDZK1 in hepatocellular carcinoma progression and the underlying PI3K/Akt signaling mechanism. *Cell. Div.* **19**, 9 (2024).
18. Chen, X. et al. HBV Infection-Related PDZK1 plays an oncogenic role by regulating the PI3K-Akt pathway and fatty acid metabolism and enhances immunosuppression. *J. Immunol. Res.* **2022**, 8785567 (2022).
19. Liu, Q., Shi, Z., Liu, X. & Xiao, H. Correlation between the coexpression of zinc finger and SCAN domain-containing protein 31 and transcriptional activator with PDZ-binding motif and prognosis in hepatocellular carcinoma. *Ann. Transl. Med.* **8**, 1308 (2020).
20. Huang, X. et al. Circ ubiquitin-like-containing plant homeodomain and RING finger domains protein 1 increases the stability of G9a and ubiquitin-like-containing plant homeodomain and RING finger domains protein 1 messenger RNA through recruiting eukaryotic translation initiation factor 4A3, transcriptionally inhibiting PDZ and homeobox protein domain protein 1, and promotes the metastasis of hepatocellular carcinoma. *J. Gastroenterol. Hepatol.* **39**, 596–607 (2024).
21. Benhammou, J. N., Sinnett-Smith, J., Pisegna, J. R. & Rozengurt, E. J. Interplay between fatty acids, Stearoyl-Co-A desaturase, mechanistic target of Rapamycin, and Yes-Associated protein/transcriptional coactivator with PDZ-Binding motif in promoting hepatocellular carcinoma. *Gastro Hep Adv.* **2**, 232–241 (2023).
22. Wang, Z. et al. Dihydromyricetin reverses MRP2-induced multidrug resistance by preventing NF-kappaB-Nrf2 signaling in colorectal cancer cell. *Phytomedicine* **82**, 153414 (2021).
23. Wang, Z. et al. Dihydromyricetin reverses MRP2-mediated MDR and enhances anticancer activity induced by oxaliplatin in colorectal cancer cells. *Anticancer Drugs.* **28**, 281–288 (2017).
24. Su, Z. et al. Silencing MRP1-4 genes by RNA interference enhances sensitivity of human hepatoma cells to chemotherapy. *Am. J. Transl Res.* **8**, 2790–2802 (2016).
25. Ostlund, T. et al. Novel EGFR-MAPK kinase and ABC transporter inhibitors for HepG2 resistant to erlotinib. *Drug Dev. Res.* **84**, 200–210 (2023).
26. Di Giacomo, S. et al. Chemosensitization of hepatocellular carcinoma cells to Sorafenib by beta-caryophyllene oxide-induced Inhibition of ABC export pumps. *Arch. Toxicol.* **93**, 623–634 (2019).
27. Zhou, M. et al. Mortality, morbidity, and risk factors in China and its provinces, 1990–2017: a systematic analysis for the global burden of disease study 2017. *Lancet* **394**, 1145–1158 (2019).

28. Yang, Y. et al. NHERF4 hijacks Mas-mediated PLC/AKT signaling to suppress the invasive potential of clear cell renal cell carcinoma cells. *Cancer Lett.* **519**, 130–140 (2021).
29. Chaouche-Mazouni, S. et al. Claudin 3, 4, and 15 expression in solid tumors of lung adenocarcinoma versus malignant pleural mesothelioma. *Ann. Diagn. Pathol.* **19**, 193–197 (2015).
30. Watanabe, M. et al. CLDN15 is a novel diagnostic marker for malignant pleural mesothelioma. *Sci. Rep.* **11**, 12554 (2021).
31. Bruno, R. et al. Gene expression analysis of biphasic pleural mesothelioma: new potential diagnostic and prognostic markers. *Diagn. (Basel)* **2022**, 12 (2022).
32. Bujko, M. et al. Expression changes of cell-cell adhesion-related genes in colorectal tumors. *Oncol. Lett.* **9**, 2463–2470 (2015).
33. Alghamdi, R. A. & Al-Zahrani, M. H. Identification of key Claudin genes associated with survival prognosis and diagnosis in colon cancer through integrated bioinformatic analysis. *Front. Genet.* **14**, 1221815 (2023).
34. Thomann, S. et al. YAP-induced Ccl2 expression is associated with a switch in hepatic macrophage identity and vascular remodelling in liver cancer. *Liver Int.* **41**, 3011–3023 (2021).
35. Lin, Z. Y., Chuang, Y. H. & Chuang, W. L. Cancer-associated fibroblasts up-regulate CCL2, CCL26, IL6 and LOXL2 genes related to promotion of cancer progression in hepatocellular carcinoma cells. *Biomed. Pharmacother.* **66**, 525–529 (2012).
36. Chen, Q. et al. Integrating single-cell and Spatial transcriptomics to elucidate the crosstalk between cancer-associated fibroblasts and cancer cells in hepatocellular carcinoma with spleen-deficiency syndrome. *J. Tradit Complement. Med.* **14**, 321–334 (2024).
37. Dia, M. et al. The long noncoding RNA TPTE2P. 1 Promotes the viability of colorectal cancer cells. *J. Cell. Biochem.* **125**, e30546 (2024).
38. Peng, L., Gao, S., Bai, F., An, Y. & Wan, F. LncRNA TPTE2P1 promotes the proliferation of thyroid carcinoma by inhibiting miR-520c-3p. *Panminerva Med.* **62**, 69–71 (2020).
39. Lv, W. et al. Downregulation of TPTE2P1 inhibits migration and invasion of gallbladder Cancer cells. *Chem. Biol. Drug Des.* **86**, 656–662 (2015).
40. Liu, J. et al. Long noncoding RNA TPTE2P1 promotes the migration and invasion of hepatocellular carcinoma. *Eur. Rev. Med. Pharmacol. Sci.* **23**, 3733–3741 (2019).
41. Liu, Y. et al. Identification and validation of a novel tertiary lymphoid Structures-Related prognostic gene signature in hepatocellular carcinoma. *World J. Oncol.* **15**, 695–710 (2024).
42. Wang, Y. et al. Noninvasive urinary protein signatures combined clinical information associated with microvascular invasion risk in HCC patients. *BMC Med.* **21**, 481 (2023).
43. Chen, J., Chen, C., Tao, L., Cai, Y. & Wang, C. A comprehensive analysis of the potential role of necroptosis in hepatocellular carcinoma using single-cell RNA seq and bulk RNA seq. *J. Cancer Res. Clin. Oncol.* **149**, 13841–13853 (2023).
44. Matsushima-Nishiwaki, R., Yamada, N., Fukuchi, K. & Kozawa, O. Sphingosine 1-phosphate (S1P) reduces hepatocyte growth factor-induced migration of hepatocellular carcinoma cells via S1P receptor 2. *PLoS One* **13**, e0209050 (2018).
45. Yoshida, T. et al. Blocking sphingosine 1-phosphate receptor 2 accelerates hepatocellular carcinoma progression in a mouse model of NASH. *Biochem. Biophys. Res. Commun.* **530**, 665–672 (2020).
46. Luo, J. et al. Mechanism of prognostic marker SPOCK3 affecting malignant progression of prostate cancer and construction of prognostic model. *BMC Cancer.* **23**, 741 (2023).
47. Zhu, S. et al. Low expression of VSIG4 is associated with poor prognosis in hepatocellular carcinoma patients with hepatitis B infection. *Cancer Manag Res.* **10**, 3697–3705 (2018).
48. Nies, A. T. et al. Expression of the multidrug resistance proteins MRP2 and MRP3 in human hepatocellular carcinoma. *Int. J. Cancer.* **94**, 492–499 (2001).
49. Zollner, G. et al. Hepatobiliary transporter expression in human hepatocellular carcinoma. *Liver Int.* **25**, 367–379 (2005).
50. Chen, W. et al. Bile acids promote the development of HCC by activating inflammasome. *Hepatol. Commun.* **;7**, 563 (2023).
51. Liang, M. et al. Ultrasound-Assisted extraction of atractylodes chinensis (DC.) Koidz. Polysaccharides and the synergistic antigastric Cancer effect in combination with oxaliplatin. *ACS Omega* **9**, 18375–18384 (2024).
52. Hegedus, T. et al. C-terminal phosphorylation of MRP2 modulates its interaction with PDZ proteins. *Biochem. Biophys. Res. Commun.* **302**, 454–461 (2003).
53. Kocher, O. et al. PDZK1, a novel PDZ domain-containing protein up-regulated in carcinomas and mapped to chromosome 1q21, interacts with cMOAT (MRP2), the multidrug resistance-associated protein. *Lab. Invest.* **79**, 1161–1170 (1999).
54. Xiang, D. et al. Upregulation of PDZK1 by Calculus Bovis sativus May play an important role in restoring biliary transport function in intrahepatic cholestasis. *Evid. Based Complement. Alternat Med.* **2017**, 1640187 (2017).

Acknowledgements

Author contributions

Zeqi Duan designed the project; Zeqi Duan performed most of the experiments; Jinyu Li, Chao Ren, Yi Chen, Duiping Feng performed a small portion of the experiments; Zeqi Duan and Chunjuan Zhao analyzed the data. Zeqi Duan and Chunjuan Zhao wrote the manuscript. Yanbo Ma and Chunjuan Zhao modified the manuscript. All authors read and approved the final manuscript.

Funding

Competing interests

The authors declare no competing interests.

Institutional review board statement

All animal experiments were conducted in strict adherence to the "Guide for the Care and Use of Laboratory Animals" issued by the National Institutes of Health and were granted approval by the Animal Ethics Committee of Shanxi Medical University (Authorization Number: DWYJ-2023-016).

Additional information

Supplementary Information The online version contains supplementary material available at https://doi.org/10.1038/s41598-025-98085-x.

Correspondence and requests for materials should be addressed to Y.M. or C.Z.

Reprints and permissions information is available at www.nature.com/reprints.

Publisher's note Springer Nature remains neutral with regard to jurisdictional claims in published maps and institutional affiliations.